International Journal of Applied Electromagnetics and Mechanics 55 (2017) 613–624
DOI 10.3233/JAE-170092
IOS Press

A fuzzy position controller for linear switched reluctance motor

J.F. Pan[a], Qianlong Li[a], Li Qiu[a], Norbert Cheung[b], Xiaoyu Wu[a] and Bo Zhang[a,*]
[a]*Laboratory of Space Collaborative Manipulation Technology, Shenzhen University, Shenzhen, Guangdong, China*
[b]*Department of Electrical Engineering, The Hong Kong Polytechnic University, Hong Kong, China*

Abstract. A fuzzy position controller is employed for the linear switched reluctance motor. Performance comparison between the fuzzy controller and a proportional-differential (PD) controller is carried out. Under the PD controller, the absolute steady-state error is 44.5 $\sim$ 211.5 μm under normal condition and 1157–1212 μm under sustained time-variant disturbance circumstance, respectively. The absolute steady-state error of 3 μm and 9 μm can be achieved under the fuzzy controller in the normal and sustained disturbed circumstance. Experimental results demonstrate that the position tracking performance from the proposed algorithm is superior to the conventional PD control strategy, both in normal circumstance and disturbance environment.

Keywords: Position control, fuzzy controller, PD controller, linear switched reluctance motor, disturbance

1. Introduction

The linear switched reluctance motor (LSRM) has a simple structure. It is rugged, reliable and low in cost. It is also suitable for operating in hostile environment. Therefore, the switched reluctance machine is an attractive candidate for position or velocity control applications [1]. Compared with rotary motor coupled with rotary-to-linear mechanical translator, a LSRM has a quicker response, a higher sensitivity, and a higher tracking precision [2]. Compared to the direct drive permanent magnet linear synchronous motor, the LSRM has a simpler and rugged structure with a lower system cost, and it does not involve the complicated arrangement of windings or permanent magnets [1]. However, a LSRM is difficult to control and its output has a higher force ripple due to its complexity and nonlinearity of the LSRM magnetic circuit. In recent years, with the development of advanced modeling and control methods, the LSRM has attracted much attention in the high-performance motion control area, and there have been reported on different aspects of LSRM. The design schemes and analysis for LSRM are presented in [2,3]. In [4], a proportional-integral (PI) controller is employed to current control for LSRM. Speed control for LSRMs is discussed in [5]. A passivity-based control (PBC) algorithm is proposed for the position tracking system of LSRM in [6]. In [7], it proposes a simple yet effective position controller that uses a lookup table to linearize the relationship among phase force, current and position, and a plug-in compensator to improve system robustness. In [8], neural networks are used to model the nonlinear functions

*Corresponding author: Bo Zhang, 3688, Nanhai Road, Shenzhen University, Shenzhen, Guangdong, China. Tel.: +86 0755 26535382; Fax: +86 0755 26557471; E-mail: zhangbo@szu.edu.cn.

for H_∞ control problems. Article [9] employs a two-degree-of-freedom controller to achieve a better tracking performance in frequency domain. These control methods can be successfully implemented on the LSRMs based on their static models. However, with the proposed algorithms above, controller parameters can not be adjusted online to counteract system uncertainties and external load disturbances, since a static machine model is considered.

A self-tuning regulator (STR) and adaptive control methods [10–12] can be proposed to combat the difficulties and uncertain control behaviors of the LSRM according to dynamic models of LSRMs. Though STR or adaptive control can achieve higher control performance, when the machine is under disturbances, the STR or adaptive controller requires a system identification process to calculate model parameters in real time [10]. The converging time for the identification process usually takes for 2–5 seconds for settling, depending on different LSRMs models and reference signals. In addition, the control system must be consistently excited to ensure the parameters to converge [11]. Therefore, a traditional PID position controller should often be involved initially for the excitation and parameter identification process [12]. Then it can be switched to the STR or adaptive control until all the above process is accomplished.

Advanced position control algorithms often increase more calculation time and storage load of the processor and sometimes, this may prevent the successful implementation onto a cost effective chip for real-time industrial applications. Regarding to the aspects of easy implementation and effectiveness of control methods, traditional PID controllers dominate more than 95% motion control applications in industry. Since the algorithm solely aims at a static linear model, the control parameters cannot be adjusted with the change of the control object after they are confirmed. Actually, the position control of a LSRM is nonlinear, time-varying, and sometime involved with dynamic interferences, etc. Therefore, parameters of the entire control structure should change with the environment and the control object. Fuzzy control imitates human control experiences rather than relies on the model of control object [13]. The algorithm has good robustness and strong ability for fault tolerance. Thus, it is a better choice for this nonlinearities and large disturbances. In this paper, a fuzzy control strategy is proposed for the LSRM for position control.

The organization of this paper is as follows: construction and modeling of the LSRM are given in Section 2, and the fuzzy PD control design is depicted in Section 3. Sections 4 and 5 present the experimental results and the conclusions, respectively.

2. Construction and modeling of the LSRM

2.1. Configuration of LSRM

The schematic and appearance of the LSRM are shown in Fig. 1a and b, respectively. The movers are composed of windings and iron cores. A set of three-phase movers are mounted on an aluminum board. The three phases have the same dimensions and ratings. The moving platform consists of three movers and the aluminum board, so that both of the total weight and inertia of the moving platform are low. The magnetic paths are decoupled [14]. The stator track and the iron cores of the mover are laminated with 0.5-mm silicon-steel plates. A linear optical position encoder with the resolution of 1 μm is mounted onto the LSRM stator track to record the motion profile of the moving platform and to feedback real-time position information. The electrical and mechanical parameters of the LSRM are listed in Table 1.

Table 1
Specifications of the LSRM

Parameter	Value
Rated power	240 W
Mass of moving platform (M)	1.5 kg
Mass of stator (M_s)	2 kg
Pole width (w_1)	6 mm
Pole pitch (w_2)	12 mm
Phase separation (g)	10 mm
Phase resistance (R)	2 ohm
Air gap length (z)	0.3 mm
Number of turns for each winding (N)	160
Stator track width	25 mm

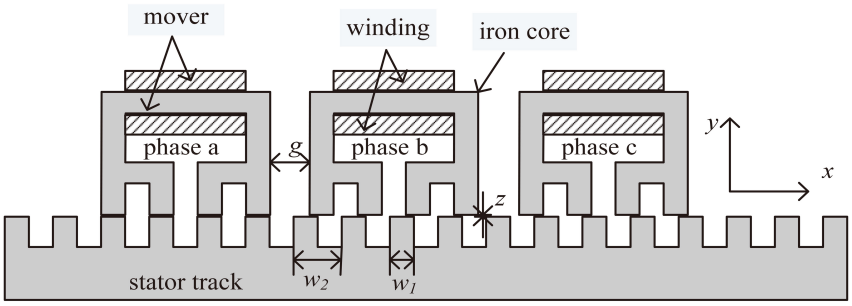

(a)

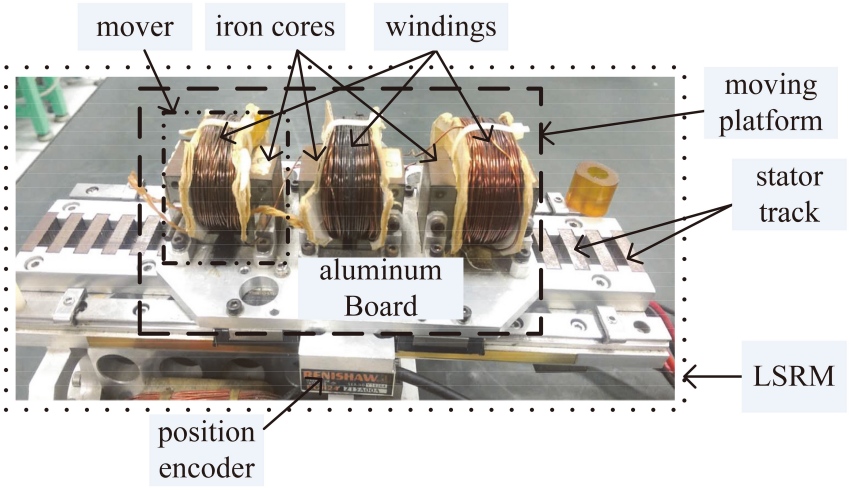

(b)

Fig. 1. Schematic (a) and picture (b) of the LSRM.

2.2. *Modeling of LSRM*

The electrical terminal for each phase can be characterized as the voltage balancing equation as follows [15],

$$u_j = R_j \cdot i_j + \frac{d\lambda_j(i_j, x)}{dt}, \quad j = a, b, c \tag{1}$$

Table 2
FDF scheme

Position range	Positive force command	Negative force command
0 mm–2 mm	$f_a = f_e$	$f_c = f_e * t_c^2/(t_c^2 + t_b^2), f_b = f_e * t_b^2/(t_c^2 + t_b^2)$
2 mm–4 mm	$f_a = f_e * t_a^2/(t_a^2 + t_c^2), f_c = f_e * t_c^2/(t_a^2 + t_c^2)$	$f_b = f_e$
4 mm–6 mm	$f_c = f_e$	$f_b = f_e * t_b^2/(t_b^2 + t_a^2), f_a = f_e * t_a^2/(t_b^2 + t_a^2)$
6 mm–8 mm	$f_c = f_e * t_c^2/(t_c^2 + t_b^2), f_b = f_e * t_b^2/(t_c^2 + t_b^2)$	$f_a = f_e$
8 mm–10 mm	$f_b = f_e$	$f_a = f_e * t_a^2/(t_a^2 + t_c^2), f_c = f_e * t_c^2/(t_a^2 + t_c^2)$
10 mm–12 mm	$f_b = f_e * t_b^2/(t_b^2 + t_a^2), f_a = f_e * t_a^2/(t_b^2 + t_a^2)$	$f_c = f_e$

note: $t_a = \sin(2\pi * x/12 + \pi/3), t_b = \sin(2\pi * x/12), t_c = \sin(2\pi * x/12 - \pi/3)$.

where R_j, u_j and i_j represent the resistance, terminal voltage and current of phase j, respectively. x is displacement and $\lambda_j(i_j, x)$ denotes the phase flux-linkage of phase j. From the mechanical side,

$$f_e = M \cdot \frac{d^2x}{dt^2} + B \cdot \frac{dx}{dt} + f_l = \sum_{j=a}^{c} \frac{\partial W_{coj}(i_j, x)}{\partial x}, \quad j = a, b, c \tag{2}$$

where f_e is the generated electromagnetic force, f_l, M and B are the external load force, mass of moving platform and friction coefficient, respectively. Co-energy $W_{coj}(i_j, x)$ can be represented as,

$$W_{coj}(i_j, x) = \int_0^{i_j} \lambda_j(i_j, x) di_j = \int_0^{i_j} L_j(i_j, x) \cdot i_j di_j, \quad j = a, b, c \tag{3}$$

It is clear that phase inductance L_j is a function respective to both phase current and displacement. The phase propulsion force can be represented as,

$$f_j(x, i_j) = \frac{\partial W_{coj}(i_j, x)}{\partial x}|_{i=\text{constant}}, \quad j = a, b, c \tag{4}$$

If the LSRM is operating under unsaturated region, the propulsion force for each phase can be denoted as,

$$f_j(x, i_j) = \frac{1}{2} \cdot \frac{dL_j}{dx} \cdot i_j^2, \quad j = a, b, c \tag{5}$$

where f_j is the generated electromagnetic force of phase j, dL_j/dx is the inductance change rate of phase j. Equation (5) indicates that the change rate of inductance respective to position and current are the key factors for propulsion force outputs and variations. The propulsion force is given by the slope of the inductance vs. motor position characteristic, and the propulsion force is proportional to the square of the current [15].

From the above deductions, the LSRM has a highly nonlinear characteristic due to its nonlinear flux behavior. Generally, the motor winding excitation scheme for LSRMs can be considered as a force distribution function (FDF) and an approximated function of the inductance change rate and the scheme of the driver can be shown in Fig. 2 [11]. FDF is used to compute the force for each phase according to the position and the direction. The approximated function of inductance change rate is used to compute the phase current according to the command force of phase and the position [11,12]. If the FDF and the approximated function of inductance change rate are chosen, then current can be calculated by the inverse function $f_j^{-1}(x, i_j)$ of Eq. (5) with the command force and its position.

In this paper, the FDF is chosen as shown in Table 2 [8] and the approximated function of the change rate of inductance is described as [16],

$$\frac{dL_j(x_j(t))}{dx_j(t)} = -K_{pj} \sin\left(\frac{2\pi x_j(t)}{w_2}\right), \quad j = a, b, c$$

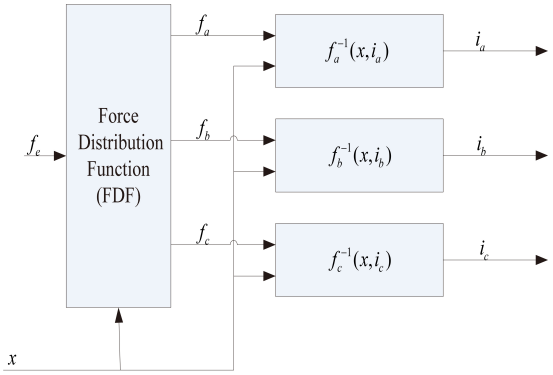

Fig. 2. Diagram of winding excitation scheme.

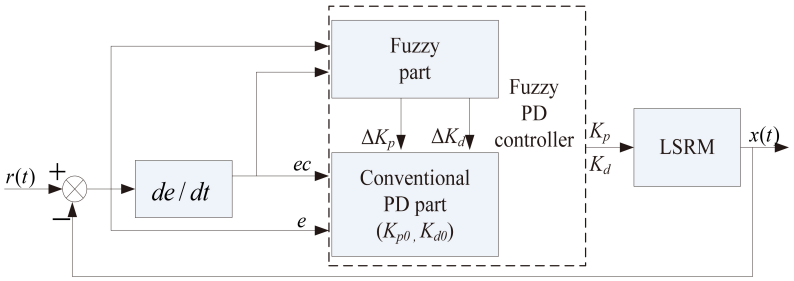

Fig. 3. Control diagram of the fuzzy PD controller.

$$x_b = x_a + \frac{2w_2}{3}$$
$$x_c = x_a + \frac{w_2}{3} \tag{6}$$

Here, w_2, x_j, and K_{pj} are the pole pitch of the LSRM, the displacement of phase j and a proportional parameter, respectively.

3. Fuzzy PD controller design

The fuzzy controller consists of a fuzzy controller and a conventional PD controller. The fuzzy PD control diagram is shown in Fig. 3. The fuzzy controller provides real-time increment values (ΔK_p, ΔK_d) to adjust the parameters of the conventional PD controller online based on the fuzzy rules and reasoning. The adjusted parameters are K_p and K_d, which are the proportional and differential gains of the fuzzy PD controller, respectively. The initial proportional and differential gains are K_{p0} and K_{d0}, and they can be regulated once. The initial gains cannot be modified after the control process starts.

The proposed fuzzy PD controller has two inputs and two outputs. The value of deviation e and the value of deviation change rate ec are the inputs for each component controller. ΔK_p and ΔK_d are the fuzzy controller outputs. The algorithm to obtain the current PD gain values can thus be briefly represented as,

$$\begin{cases} K_p = K_{p0} + \Delta K_p \\ K_d = K_{d0} + \Delta K_d \end{cases} \tag{7}$$

Table 3
Fuzzy rule

$\Delta K_p \backslash \Delta K_d$ / e \ ec	NB	NM	NS	ZO	PS	PM	PB
NB	PB\PS	PB\PS	PM\PB	PM\PB	PS\PM	PS\PS	ZO\PS
NM	PB\PS	PB\PS	PM\PB	PS\PM	PS\PM	ZO\PS	ZO\ZO
NS	PM\ZO	PM\PS	PM\PM	PS\PM	ZO\PS	ZO\PS	ZO\ZO
ZO	PM\ZO	PM\PS	PS\PS	ZO\PS	PS\PS	PM\PS	PM\ZO
PS	ZO\ZO	ZO\PS	ZO\PS	PS\PM	PS\PM	PM\PS	PM\ZO
PM	ZO\ZO	ZO\PS	PS\PM	PS\PM	PM\PB	PM\PS	PB\PS
PB	ZO\PS	PS\PS	PM\PM	PM\PB	PM\PB	PB\PS	PB\PS

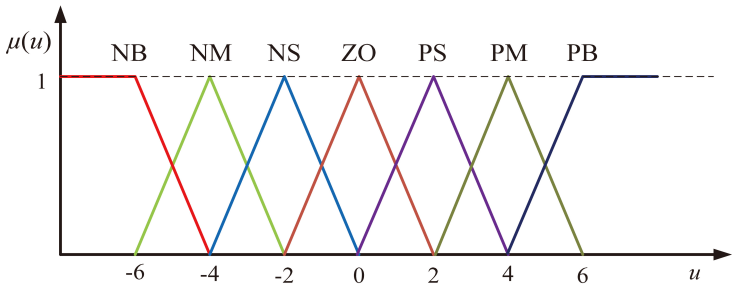

Fig. 4. Membership functions for inputs and outputs.

Detailed information to derive ΔK_p and ΔK_d can be summarized as the following steps.

The fuzzification process is to transform the accurate input values into a set of fuzzy variables. Both of the transformed input and output domains of fuzzy set are selected as $[-6\ -4\ -2\ 0\ 2\ 4\ 6]$. The fuzzy sets for inputs and outputs contain the same fuzzy linguistic variables as: {Negative Large (NL), Negative Middle (NM), Negative Small (NS), Zero (ZO), Positive Small (PS), Positive Middle (PM), Positive Big (PB)}. A symmetric, equi-distribution, full-fold triangular membership function are employed for all input and output variables and the membership functions are shown in Fig. 4. The horizontal coordinate μ is the value of input variable after domain transformation. The longitudinal coordinate $\mu(u)$ is the membership function of the input variable.

The setting rule table for fuzzy reasoning is shown in Table 3. The rule table is obtained according to the following principles which are summarized from the different roles of the proportional and differential parameters [13].

(1) When e is large, we can set a larger K_p and a smaller K_d to achieve a good dynamic response performance and reduce error rapidly.
(2) When e is medium, a small size K_p and a medium size K_d can be set to reduce error and to prevent big overshoot from the position response.
(3) When e is small, in order to further reduce error, overcome overshoot and make the system stable rapidly, K_p should be reduced continuously.
(4) The error change rate indicates the changing speed of error, as well as the speed of response. In order to avoid system oscillation, the value selections of K_d should refer to the value of ec. When the value of ec is small, the value of K_d can be large, when the value of ec is large, the value of K_d can be small, usually, it is set as a medium value.

The input values e and ec are continuously detected in the control process. Then they are transformed into two numbers in the scope of input domain and they are given the corresponding linguistic variables according to Fig. 4. Finally, the fuzzy reasoning results can be obtained from the basis of Table 3.

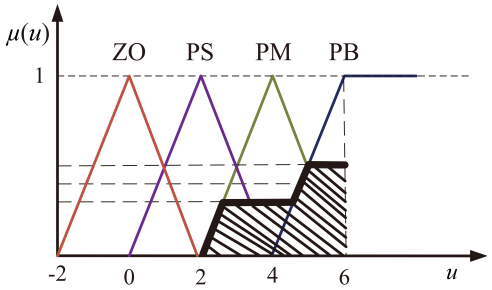

Fig. 5. Membership functions obtained from Mamdani inference.

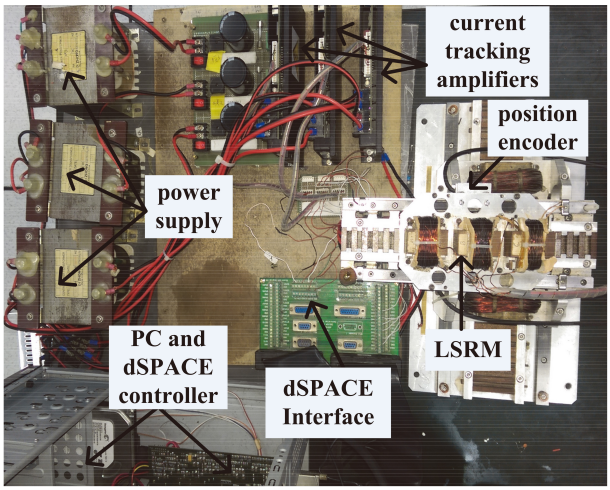

Fig. 6. Experimental setup.

Defuzzification is introduced to translate the fuzzy reasoning results into clear values, which can be directly used for practical control. ΔK_p and ΔK_p are generated on-line according to the fuzzy control rules to compensate K_p and K_p for meeting the control requirements. In this paper, the Mamdani inference is selected as the fuzzy inference method [13]. It contains three processes, the aggregation, activation and accumulation of membership function. The area center of gravity method is adopted as defuzzification strategy. The expression is denoted as,

$$u^* = \frac{\int_{\text{MIN}}^{\text{MAX}} u \cdot \mu(u) du}{\int_{\text{MIN}}^{\text{MAX}} \mu(u) du} \tag{8}$$

where u^* is the defuzzification output value, u is the independent variable of membership function domain. $\mu(u)$ is the membership function accumulated from Mamdani inference method as the black bold line shown in Fig. 5. [MIN, MAX] is the domain of the $\mu(u)$. The enclosed area by $\mu(u)$ polyline and u axis is the integral area which is shadowed in Fig. 5.

4. Experimental results

The experimental setup is shown in Fig. 6. The computer is a Pentium 4 personal computer that is used to download the target codes into a dSPACE DS1104 controller card. The control algorithm is developed

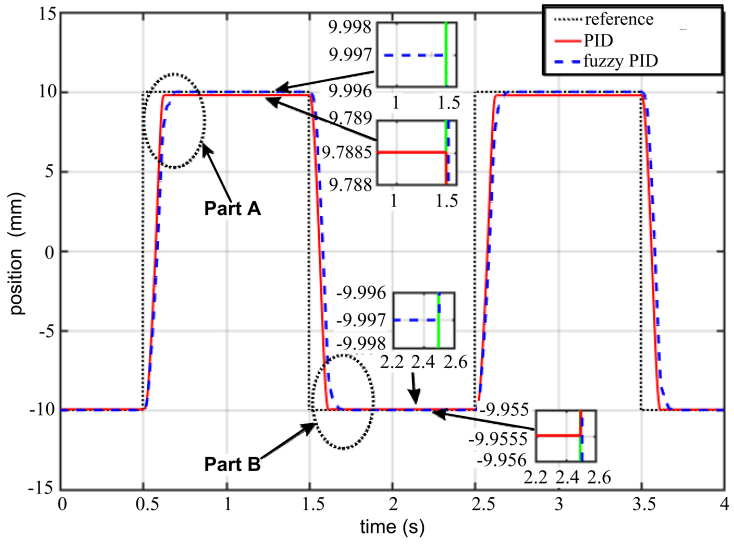

Fig. 7. Profiles of position responses under conventional PD and fuzzy controller.

under the *MATLAB/SIMULINK* environment and all control functions are implemented by the dSPACE DS1104 card. For the current tracking amplifier, the commercial drivers consist of three asymmetric bridge inverters with 90 VDC power supply. A linear optical position encoder is mounted on the moving platform of the LSRM system and providing position feedback information.

The optimal values of K_{p0} and K_{d0} are adjusted under the conventional PD controller according to the trial and error basis. K_{p0} and K_{d0} are 12 and 0.16, respectively. The PID parameters are configured such that a minimum steady-state error values can be achieved under the nominal position reference signal of 10 mm amplitude and 0.5 Hz of frequency.

Figure 7 shows the position tracking waveforms and its corresponding control signal waveform under the conventional PD controller and the proposed fuzzy PD controller, respectively. It can be seen that the fuzzy PD controller behaves a good tracking performance both in positive period and negative period. However, the conventional PD controller presents an obvious asymmetric tracking performance.

Figure 8a and b are the partial enlarged details of Part A and Part B in Fig. 7, respectively. Figure 8a and b show the rise time and accommodation time of the position tracking system in positive period and negative period respectively under different controllers. In the positive period, the rise time and accommodation time under the conventional PD controller are 0.608 s and 0.627 s, respectively. The rise time and accommodation time under the fuzzy PD controller are 0.620 s and 0.673 s. In the negative period, the drop time and accommodation time under the conventional PD controller are about 1.595 s and 1.610 s, respectively. The drop time and accommodation time under the fuzzy PD controller are 1.620 s and 1.665 s, respectively.

Figure 9 shows the profiles of steady-state error under the conventional PD controller and the fuzzy PD controller. From Fig. 9, it can be seen that the conventional PD controller can achieve a 211.5 μm and 44.5 μm steady-state error in the positive period and negative period, respectively. However, the fuzzy PD controller can achieve the steady-state error of $\pm$ 3 μm.

Figure 10 shows the position tracking waveforms and its corresponding control signal waveform under the control of the proposed fuzzy PD controller and a conventional PD controller respectively, with a 100 N/m spring mounted on one side of the moving platform. Figure 11 illustrates the profiles of steady-state error under the conventional PD controller and fuzzy PD controller with the spring. According

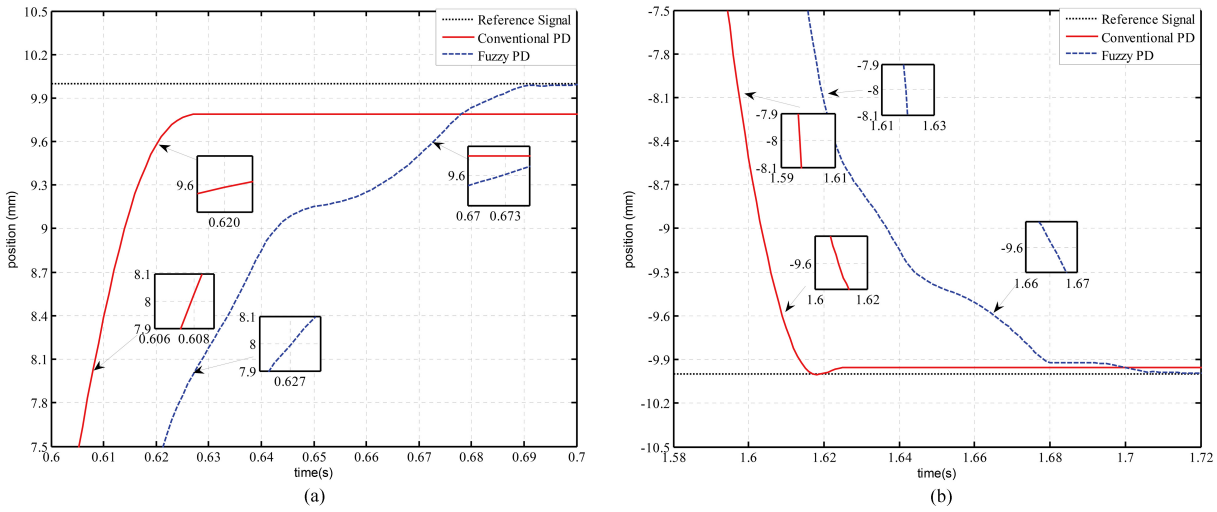

Fig. 8. Profiles of rise time and accommodation time in positive period (a) and negative period (b) under different controllers.

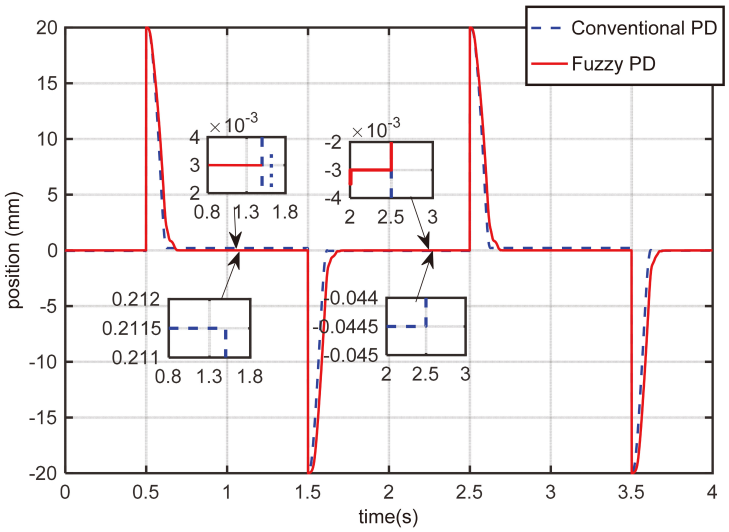

Fig. 9. Profiles of steady-state error under conventional PD and fuzzy PD controller.

to Fig. 11, when a sustained turbulence is loaded to LSRM, the position tracking curve appears an obvious increased steady-state error under the conventional PD controller. However the position tracking curve under the fuzzy PD controller performs a good steady-state error. Figure 11 clearly shows that the steady-state errors are controlled in the range from 1157–1212 μm and the range from 8–9 μm under the conventional PD controller and the fuzzy PD controller, respectively.

The key control indices from the experiment results are collected in Table 4. It is clearly that the steady-state errors between the positive period and negative period are quite different under the conventional PD controller. This is because the mathematic models from the positive and negative period are not uniform, and the reason may originate from the asymmetric behaviors such as friction coefficients or manufacture imperfection, etc. Nevertheless, the steady-state error between positive period and negative

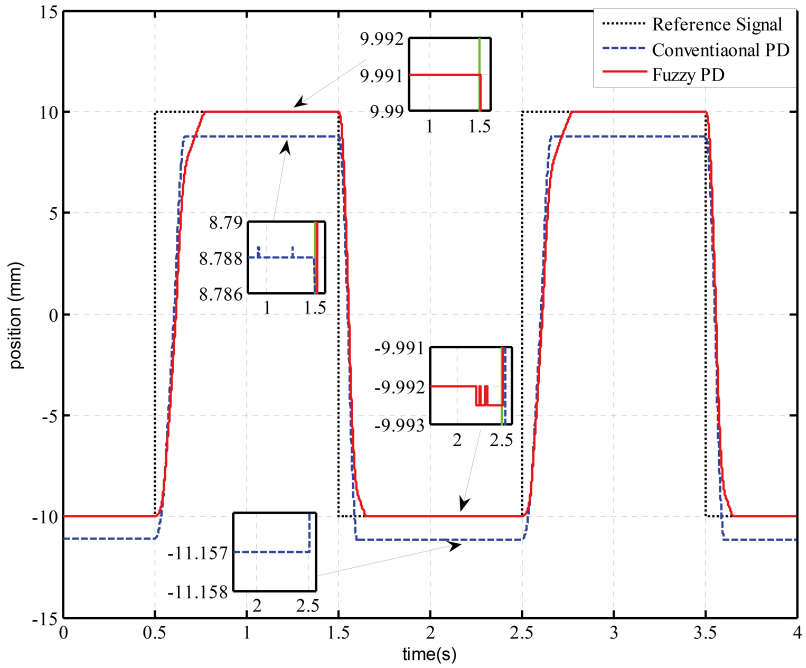

Fig. 10. Profiles of position responses with a spring load under conventional PD and fuzzy controller.

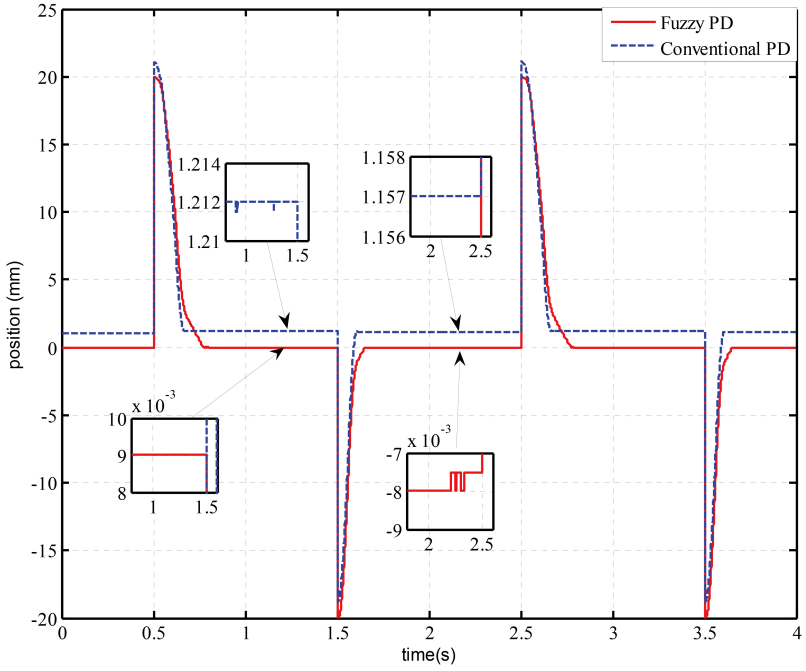

Fig. 11. Profiles of steady-state error with a spring load under conventional PD and fuzzy controller.

Table 4
Results of control indices

Stage	Items	Convention PD controller	Fuzzy PD controller
Positive period	Rise time	0.608 s	0.620 s
	Accommodation time	0.627 s	0.673 s
	Steady-state error (no spring)	211.5 μm	3 μm
	Steady-state error (with spring)	1212 μm	9 μm
Negative period	Rise time	1.595 s	1.620 s
	Accommodation time	1.610 s	1.665 s
	Steady-state error(no spring)	-44.5 μm	-3 μm
	Steady-state error(with spring)	1157 μm	-8 μm

period are almost symmetric under the fuzzy PD controller both in the normal circumstance without disturbance and sustained disturbed circumstance. Though sacrificing little dynamic performance, the fuzzy PD controller can compensate the influence of the model variations. It can obtain a good steady-state capability especially under sustained disturbance.

5. Conclusion

This paper proposes a fuzzy PD control method for the high-precision control of the LSRM. Experimental results demonstrate that the steady-state errors of the position tracking for the LSRM in the positive and negative period can maintain symmetric, and the steady-state errors can be maintained within $\pm$ 10 μm when the system parameters are under the external disturbance. These results confirm that the method is effective and robust in the position tracking for the LSRM.

The proposed fuzzy PD has the merit to increase the steady-state error precision, however, the rise time is sacrificed for the steady-state regulation based on the fuzzy algorithm.

Acknowledgments

This work was supported by the National Natural Science Foundation of China under Grant 51477103, 51577121 and 51575360, and in part by the Guangdong Natural Science Foundation under Grant S2014A030313564, 2015A010106017 and 2016KZDXM007. The authors also would like to thank Shenzhen Government under code JCYJ20160308104825040 for support.

References

[1] J.-H. Choi, J. Lee and Y.-H. Kim, Geometric Design of Pole Arcs Considering Electric Parameters in Switched Reluctance Motor, *International Journal of Applied Electromagnetics and Mechanics* **19**(1–4) (2004), 275–279.

[2] A. Stuikys, M. Rotaru and J.K. Sykulski, A Refined Approach Exploiting Tubes of Flux for Analysis of Linear Switched Reluctance Motors, *International Journal of Applied Electromagnetics and Mechanics* **51**(s1) (2016), S13–S21.

[3] Q. Lu, X. Ma, X. Huang and Y. Ye, Performance investigation of odd primary pole linear switched-flux PM machine with mechanical flux adjuster, *International Journal of Applied Electromagnetics and Mechanics* **53**(4) (2017), 745–756.

[4] H.-K. Bae, B.-S. Lee, P. Vijayraghavan and R. Krishnan, A linear switched reluctance motor: converter and control, *IEEE Transactions on Industry Applications* **36**(5) (Sep/Oct 2000), 1351–1359.

[5] J.F. Pan, S.C. Kwok, N.C. Cheung and J. Yang, 'Auto disturbance rejection speed control of linear switched reluctance motor,' Fourtieth IAS Annual Meeting, in: *Conference Record of the 2005 Industry Applications Conference*, Vol. 4, 2005, pp. 2491–2497.

[6] S.W. Zhao, N.C. Cheung, W.C. Gan, J.M. Yang and Q. Zhong, Passivity-based control of linear switched reluctance motors with robustness consideration, *IET Electric Power Applications* **2**(3) (May 2008), 164–171.
[7] W.-C. Gan, N.C. Cheung and L. Qiu, Position control of linear switched reluctance motors for high-precision applications, *IEEE Transactions on Industry Applications* **39**(5) (Sept.–Oct. 2003), 1350–1362.
[8] H. Li, Y. Liu, J. Wang, Y.K. Wong and W.L. Chan, Neural networks based nonlinear H∞ control for linear switched reluctance motor, in: *Asian Control Conference, 2009. ASCC 2009. 7th*, Hong Kong, 2009, pp. 796–801.
[9] X. Sun, B. Su, L. Chen, Z. Yang, Y. Yang, W. Qiao and S. Han, A High-performance Control Scheme for Reluctance Type Bearingless Motors, *International Journal of Applied Electromagnetics and Mechanics* **53**(3) (2017), 537–549.
[10] K. Takahashi, Y. Shiotani and M. Hashimoto, Self-tuning PID Controller Using Quantum Neural Network with Qubit-inspired Neurons, *International Journal of Hybrid Intelligent Systems* **12**(1) (2015), 41–52.
[11] S.W. Zhao, N.C. Cheung, W.C. Gan and J.M. Yang, High-Precision Position Control of a Linear-Switched Reluctance Motor Using a Self-Tuning Regulator, *IEEE Transactions on Power Electronics* **25**(11) (Nov. 2010), 2820–2827.
[12] J.F. Pan, Y. Zou and G. Cao, Adaptive controller for the double-sided linear switched reluctance motor based on the nonlinear inductance modelling, *IET Electric Power Applications* **7**(1) (Jan. 2013), 1–15.
[13] S. Zhang, Y. Zhang, X. Zhang and Y. Zheng, Fuzzy PID control of doubly curved shell using MFC actuator, *International Journal of Applied Electromagnetics and Mechanics* **52**(3–4) (2016), 1277–1286.
[14] Z. Liu and Z. Deng, A Switched Reluctance Motor with Conical Magnetic Bearings, *International Journal of Applied Electromagnetics and Mechanics* **54**(2) (2017), 141–164.
[15] Q. Yu, X. Wang and Y. Cheng, Multiphysics Optimization Design Flow with Improved Submodels for Salient Switched Reluctance Machines, *International Journal of Applied Electromagnetics and Mechanics*, Preprint, no. Preprint, 2017, 1–14.
[16] A.A. Yadghar, K.M. Mokhtari and M.J. Navardi, Optimization of new geometries of switched reluctances motors using FEM and multi objective genetic algorithm, *International Journal of Applied Electromagnetics and Mechanics* **53**(2) (2017), 211–226.
[17] B.-Y. Cao, G. Wang, S. Guo and S. Chen, Fuzzy Information and Engineering 2010, Springer Berlin, Germany, 2010.